

**DOUBLE-INVERTER FED WOUND ROTOR INDUCTION MACHINE
DRIVES: CONTROL AND RIPPLE MINIMIZATION**

NIKHIL KRISHNA BAJJURI



**DEPARTMENT OF ELECTRICAL ENGINEERING
INDIAN INSTITUTE OF TECHNOLOGY DELHI**

NOVEMBER 2020

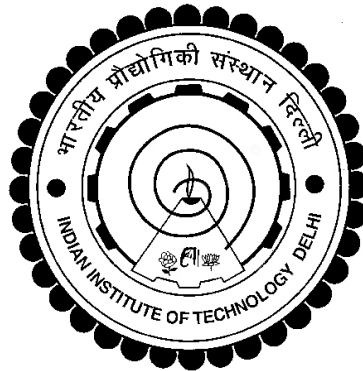
© Indian Institute of Technology Delhi (IITD), New Delhi, 2020

**DOUBLE-INVERTER FED WOUND ROTOR INDUCTION MACHINE
DRIVES: CONTROL AND RIPPLE MINIMIZATION**

by

NIKHIL KRISHNA BAJJURI
Department of Electrical Engineering

Submitted
in fulfillment of the requirements of degree of Doctor of Philosophy
to the



INDIAN INSTITUTE OF TECHNOLOGY DELHI

NOVEMBER 2020

Certificate

It is certified that the thesis entitled “**Double-Inverter fed Wound Rotor Induction Machine Drives: Control and Ripple Minimization,**” being submitted by **Mr. Nikhil Krishna Bajjuri** for award of the degree of **Doctor of Philosophy** in the Department of Electrical Engineering, Indian Institute of Technology Delhi, is a record of the student work carried out by him under my supervision. The matter embodied in this thesis has not been submitted for award of any other degree or diploma.

Dated:

(Dr. Amit Kumar Jain)
**Department of Electrical Engineering,
Indian Institute of Technology Delhi,
Hauz Khas, New Delhi-110016, India.**

Acknowledgements

It has always been a pleasure to remind all the excellent people connected, directly or indirectly, to my doctoral research.

First of all, I bow to my head in respect to **Dr. Amit Kumar Jain**, my thesis advisor, especially for imparting the first seed of knowledge on Wound Rotor Induction Machines. His patience and calmness, in all forms of life, has always surprised me. His insight and foreseeing nature has helped me in gaining the maximum out of my research life at IIT. The brain storming sessions with him will be the most cherished technical moments of my life. Apart from the doctoral research, he has been at a constant help in balancing my professional and personal life.

Second, I shall not miss this opportunity to express my indebtedness to **P. Vinod Kumar**, Asst. Prof., C.V.R College of Engineering, without whom the journey to the IIT would not have been possible. His guidance, throughout the journey of analog and power electronic circuit design, is unforgettable. The knowledge gained from the power electronic projects, carried out under his guidance, has helped me to validate my doctoral research.

Third, I thank the review committee members, **Prof. M. Veerachary**, **Dr. Ramkrishan Maheshwari**, and **Dr. Anandarup Das**, for their appreciation, suggestions, and thoughtfulness, during the progress review sessions. I would like to appreciate the laboratory facilities and research environment provided by **Dr. Ramkrishan Maheshwari**, and **Dr. Anandarup Das**. I would also like to take this opportunity to thank **Dr. Seshan Srirangarajan**, for his help in procuring the machine setup. I would also like to thank **Mr. Dhanraj Singh**, and **Late. Mr. Suresh Chand** for their constant help in consumable/non-consumable procurement and laboratory sessions.

Besides, I would like to appreciate and thank **Dr. Himanshu Misra** and **Dr. Kapil Shukla**, for their spiritual and technical discussions. Especially, the spiritual discussions have enlightened and changed my viewpoint towards the science behind Indian culture. I shall not forget the technical discussions on DSP coding with M.tech students, **Mr. Sumeet Thakur** and **Mrs. Akhila Kishore**. The technical and non-technical expeditions with **Mr. Navneet Vaishnav** will always be cherished throughout my life. The tough knowledge sharing sessions with **Dr. Prasun Mishra** have helped me in increasing my level of patience. The enlightening discussions with **Mr. Himanshu Swamy** are unforgettable. I would also take this opportunity to thank **Mr. Rishikant Sharma**, **Dr. Shailendra Kumar**, **Mr. Anshul Varshney**, and **Late Dr. Konda Srikanth Reddy** for their refreshing messing, badminton, and tea-time sessions. And, I convey my best wishes and thanks to all the lab-mates, **Mr. Rahul Sharma**, **Mrs. Nidhi Bist**, **Mrs. Nebedita Parida**, **Mr. Martin Ch.**, **Mr. Aamir Rafiq**, **Miss. Khusboo Kumari**, **Miss. Cheshta Jain**, and **Miss. Apurva Verma**.

Lastly, I bow my head in respect to my parents, **Shri. B. Rajeshwar** and **Smt. B. Chandrakala**, my elder brother, **Shri. B. Nithin Kumar**, and my family, for their constant appreciation, motivation, and sacrifice, which paved a beautiful path to my doctoral research. I find no words to express the simplest things done by my wife, **Mrs. Nandini**, which acted as stress busters. I can only thank her for bearing my absence and yet being a motivation factor to me.

The work carried out in this thesis is funded by **Vishveswaraya PhD Scheme**, Ministry of Electronics and Information Technology (MeitY), India.

(Nikhil Krishna Bajjuri)

Abstract

The presence of VSCs on the stator and rotor terminals of Double-Inverter fed Wound Rotor Induction Machine (DI-WRIM) drives add to the power handing capability and control flexibility of the drive. However, due to the stator and rotor VSCs, the control and implementation complexity as well as the harmonic content of the drive is also increased. This thesis deals with the minimization of control and implementation complexity and, the harmonic content in the DI-WRIM drives.

To minimize the control and implementation complexity, the DI-WRIM drive is modelled and controlled as '2' virtual SQIMs. In the proposed modelling and control technique of DI-WRIM as '2' virtual SQIMs, the stator and rotor side controllers are identical to conventional FOC based SQIM drives. Thus, to control the DI-WRIM drive, two FOC based SQIM drives can be directly connected to the stator and rotor terminals of the WRIM, with some external communication. The '2' virtual SQIMs must produce a common torque in the air-gap and hence, the '2' virtual SQIMs are coupled using a common medium of coupling and this medium is the load angle between the stator and rotor currents. The feasibility of the proposed modelling and control technique is presented through extensive experimental results.

Unlike in SQIM drives, the harmonic source on the rotor side of the DI-WRIM also contributes to the ripple, along with the stator side harmonic source. This ripple is superimposed on the stator and rotor, fundamental fluxes and currents and, the generated torque. Thus, the harmonic model of the DI-WRIM drive is presented, in this thesis. Similar to the ripple analysis of SQIM drives, the torque ripple and current ripple in DI-WRIM is formulated in terms of the stator and rotor flux ripples, which are estimated from their respective sides. To facilitate the open-loop estimation of torque ripple and current ripple, a rotor position (speed) independent transformation technique is also proposed, to transform the estimated flux ripples to a single flux oriented reference frame. One important aspect of the harmonic analysis is that the interaction of stator and rotor flux ripples, which form current and torque ripple, is dependent on the mode of operation of WRIM. Therefore, stator-rotor PWM combinations, formed using the available PWM techniques, are proposed to reduce the torque and current ripple. Apart from the torque and current ripple in DI-WRIM, the variation of switching loss in the stator and rotor VSCs, due to the variation of stator and rotor power factors, is also analyzed. Based on the analysis, stator-rotor PWM combinations are also proposed to solely reduce switching loss and to reduce both current ripple and switching loss, along with flux sharing schemes between stator and rotor sides. The proposed PWM combinations, which are dedicated to reduce torque ripple, current ripple and/or switching loss, are independent within each other and does not majorly effect the other ripple.

The topology of DI-WRIM resembles the topology of Double-Inverter fed Open-End Winding Induction Machine (DI-OWIM) drive. In the DI-OWIM drive, each of the two stator winding terminals are connected to two individual VSCs, with isolated dc-link. The two VSCs are switched such that a 3-Level

Neutral Point Clamped (3L-NPC) converter is emulated on the stator terminals of the OWIM, in terms of the phase voltage. Thus, the ripple in the OWIM is similar to that of a 3L-NPC converter fed SQIM (3L-SQIM). This resemblance of DI-OWIM in DI-WRIM is explored to develop Equivalent 3L (EQ-3L) stator-rotor PWM combinations such that, a 3L-NPC converter is emulated in the air-gap of the WRIM, in terms of the quadrature axes flux ripples. With the proposed EQ-3L PWM combinations, the torque ripple in DI-WRIM is equivalent to the torque ripple in 3L-SQIM drive and it is further reduced when compared to stator-rotor PWM combinations formed using available PWM techniques.

The proposed modelling and control technique, combined with the proposed stator-rotor PWM combinations, can be a solution towards high performance DI-WRIM drive.

सार

द्वि-इन्वर्टर स्रोत वाउंड-रोटर-इंडक्शन-मशीन (द्वि-इन्व.वा.रो.इं. म.) ड्राइव के स्टेटर और रोटर के अवसान पर वोल्टेज-स्रोत-कनवर्टर का होना, उसकी क्षमता शक्ति और नियंत्रण शक्ति को बढ़ाता है। लेकिन, स्टेटर और रोटर के अवसान पर वोल्टेज-स्रोत-कनवर्टर के होने से, नियंत्रण और कार्यान्वयन की जटिलता के साथ-साथ हार्मोनिक मात्रा भी बढ़ जाती है। यह थीसिस उसी नियंत्रण और कार्यान्वयन की जटिलता और हार्मोनिक मात्रा को कम करने का अध्ययन करता है।

यह कार्य नियंत्रण और कार्यान्वयन की जटिलता को कम करने के लिए द्वि-इन्व.वा.रो.इं.म. को दो अप्रत्यक्ष स्किर्रेल-केज-इंडक्शन-मशीन (स्कि.के.इं.म) के रूप में प्रतिरूपित और नियंत्रित करता है। इसके लिए प्रस्तावित किये गए प्रतिरूप और नियंत्रण शैली में स्टेटर और रोटर के तरफ के नियंत्रक एक पारंपरिक रोटर फ्लक्स उन्मुखी स्कि-के-इं-म ड्राइव के समान हैं। यह कार्य कहता है कि द्वि-इन्व.वा.रो.इं.म. ड्राइव को नियंत्रित करने के लिए, किसी बाहरी संचार के साथ दो स्कि-के-इं-म ड्राइव को सीधा द्वि-इन्व.वा.रो.इं.म. के स्टेटर और रोटर अवसान पर लगाया जा सकता है। इसके लिए जरूरी है कि दो स्कि.के.इं.म. स्टेटर और रोटर के बीच वात पर एक समान टार्क पैदा करें, और इस कारण दो अप्रत्यक्ष स्कि.के.इं.म. एक समान माध्यम से जुड़े हैं जो कि स्टेटर और रोटर के विद्युत प्रवाह के बीच का कोण है। इस कार्य की साध्यता को विस्तार से प्रयोगों द्वारा दर्शाया गया है।

स्कि.के.इं.म. ड्राइव से भिन्न, द्वि-इन्व.वा.रो.इं.म. में रोटर की तरफ का हार्मोनिक स्रोत भी स्टेटर की तरफ के हार्मोनिक स्रोत की तरह तरंगों को प्रभावित करता है। यह तरंगों स्टेटर और रोटर के विद्युत प्रवाह, फ्लक्स और उत्पन्न टार्क में संलग्न हो जाती हैं। इसीलिए, द्वि-इन्व.वा.रो.इं.म. का हार्मोनिक प्रतिरूप इस थीसिस में प्रस्तुत किया गया है। स्कि.के.इं.म. ड्राइव के तरंग विश्लेषण के समान, द्वि-इन्व.वा.रो.इं.म. टार्क तरंग और विद्युत तरंग को सुत्रित किया गया है, जिनका आंकलन उनके अपने पक्ष से किया गया है। टार्क तरंग और विद्युत प्रवाह की तरंग के ओपन-लूप आंकलन की सुविधा के मद्देनजर आंकलित फ्लक्स तरंगों को एक अकेले फ्लक्स उन्मुखी ढांचे में करने के लिए, रोटर की स्थिति से स्वतंत्र एक तकनीक भी प्रस्तावित की गई है। स्टेटर और रोटर के फ्लक्स तरंगों के मिलने से टार्क तरंग और विद्युत प्रवाह तरंग का बनना हार्मोनिक विश्लेषण का एक महत्वपूर्ण पहलू है, जो कि वा.रो.इं.म. के परिचालन पर निर्भर करता है। इसलिए, उपलब्ध पी .डब्लू. एम. तकनीक के उपयोग से टार्क तरंग और विद्युत प्रवाह के तरंगों को कम करने के लिए स्टेटर और रोटर का पी .डब्लू. एम. संयोजन प्रस्तावित किया गया है। द्वि-इन्व.वा.रो.इं.म. में टार्क तरंग और विद्युत प्रवाह के तरंगों के साथ साथ स्टेटर और रोटर में उनके पावर फैक्टर के कारण होने वाले स्विचिंग हानि का भी अध्ययन किया गया है। अध्ययन के अनुसार, सिर्फ स्विचिंग हानि कम करने के लिए और विद्युत प्रवाह के तरंगों के साथ साथ स्विचिंग हानि को कम करने के लिए स्टेटर और रोटर में पी .डब्लू. एम. संयोजन भी प्रस्तावित किये गए हैं। टार्क तरंग, विद्युत प्रवाह के

तरंग और/या स्विचिंग हानि को कम करने के लिए प्रस्तावित पी .डब्लू. एम. संयोजन एक दूसरे से भिन्न हैं और किसी दूसरे तरंग को प्रभावित नहीं करते हैं।

द्वि-इन्व.वा.रो.इं.म. की सांस्थिति एक द्वि इन्वर्टर स्रोतित ओपन-एन्ड वाइंडिंग इंडक्शन मशीन (द्वि-इन्व.-ओ.वा.इं.म.) की सांस्थिति को दर्शाती है। द्वि-इन्व.-ओ.वा.इं.म. में स्टेटर के दोनों अवसान दो पृथक वोल्टेज-स्रोत-कनवर्टर से जोड़े जाते हैं, जो कि अलग अलग डीसी-लिंक के साथ हैं। दो पृथक वोल्टेज-स्रोत-कनवर्टर की स्विचिंग इस तरह की जाती है कि वह ओ.वा.इं.म. के स्टेटर अवसान पर उपस्थित फेज-वोल्टेज के अनुसार एक 3-स्तर के न्यूट्रल-पॉइंट-क्लेमपड कनवर्टर का अनुकरण करें। इसीलिए, ओ.वा.इं.म. में तरंगों एक 3-स्तर के न्यूट्रल-पॉइंट-क्लेमपड कनवर्टर के समान होतीं हैं। द्वि-इन्व.-ओ.वा.इं.म. का द्वि-इन्व.वा.रो.इं.म. की तरह अनुसरण का अध्ययन एक समकक्ष 3-स्तर के स्टेटर-रोटर के पी .डब्लू. एम. संयोजन बनाने के लिए किया गया है। क्राडेचर- एक्सेस-प्लक्स -तरंगों के रूप में यह 3-स्तर का न्यूट्रल-पॉइंट-क्लेमपड कनवर्टर वा.रो.इं.म. के स्टेटर और रोटर के बीच वात पर उत्पादित किया गया है। प्रस्तावित 3-स्तर के पी .डब्लू. एम. संयोजन को लागू करने से टार्क तरंग एक 3-स्तर के स्क्रि.के.इं.म ड्राइव के समान होतीं हैं, और यह तरंगों उपलब्ध पी .डब्लू. एम. तकनीक के उपयोग से स्टेटर-रोटर पी .डब्लू. एम. संयोजन बनाने की अपेक्षा और कम हो जाती हैं।

प्रस्तावित कार्यान्वयन और नियंत्रण तकनीक, प्रस्तावित स्टेटर-रोटर पी .डब्लू. एम. संयोजन के साथ एक अच्छा प्रदर्शन करने वाले द्वि-इन्व.वा.रो.इं. म. ड्राइव का समाधान पेश करते हैं

Contents

| | |
|--|------------|
| Acknowledgements | v |
| Abstract | vii |
| Contents | xi |
| List of Figures | xv |
| List of Tables | xix |
| Nomenclature | xxi |
| 1 Introduction | 1 |
| 1.1 Literature on Modelling and Control of DI-WRIM drive | 3 |
| 1.2 Literature on Harmonic Distortion in SQIM drive | 4 |
| 1.2.1 Current Ripple and Switching Loss Minimization | 5 |
| 1.2.2 Torque Ripple Minimization | 6 |
| 1.3 Scope and Contributions | 7 |
| 1.3.1 Modelling and Control of DI-WRIM drive | 7 |
| 1.3.2 Ripple Minimization in DI-WRIM drive | 8 |
| 1.4 Outline of the Thesis | 9 |
| 2 Modelling, Control, and Ripple Analysis of DI-WRIM | 11 |
| 2.1 Modelling of WRIM | 11 |
| 2.1.1 Stator Flux Oriented (D - Q) Model: | 12 |
| 2.1.2 Rotor Flux Oriented (D_1 - Q_1) Model: | 13 |
| 2.1.3 Air-gap Flux Oriented (D_3 - Q_3) Model: | 14 |
| 2.2 Control of DI-WRIM | 15 |
| 2.2.1 Stator and Rotor Frequency Plots: | 16 |
| 2.2.2 Design of PI-Cs: | 18 |
| Inner PI-Cs: | 18 |
| Outer PI-C: | 19 |
| 2.2.3 Vector Diagram of DI-WRIM: | 20 |
| In Sub-Synchronous Mode | 20 |
| In Super-Synchronous Mode | 20 |
| 2.3 Ripple Analysis of DI-WRIM | 21 |
| 2.3.1 Formulation of Torque Ripple: | 22 |
| 2.3.2 Formulation of Current Ripple: | 23 |
| 2.3.3 Speed Independent Transformation: | 23 |
| 2.3.4 Torque Ripple in Stator Flux (D - Q) Frame: | 24 |
| 2.3.5 Current Ripple in Stator Flux (D - Q) Frame: | 25 |
| 2.3.6 Harmonic Equivalent Circuit of DI-WRIM: | 26 |
| 2.4 Conclusion | 27 |

| | | |
|----------|---|-----------|
| 3 | Proposed Modelling and Control of DI-WRIM as ‘2’ Virtual SQIMs | 29 |
| 3.1 | Analysis of WRIM as ‘2’ Virtual SQIMs | 30 |
| 3.2 | Mathematical Model of DI-WRIM as ‘2’ Virtual SQIMs | 31 |
| 3.2.1 | Stator Side Model: | 31 |
| 3.2.2 | Rotor Side Model: | 32 |
| 3.2.3 | Torque Equation: | 33 |
| 3.3 | Current Oriented Control Technique | 33 |
| 3.3.1 | Stator Side Controller: | 33 |
| 3.3.2 | Rotor Side Controller: | 34 |
| 3.3.3 | Generalized Flux Sharing Scheme: | 34 |
| 3.3.4 | Starting Method of the Drive: | 36 |
| 3.3.5 | Generation of Transformation Angles: | 36 |
| 3.3.6 | Limits on Current PI-Cs: | 37 |
| 3.4 | Experiment Results and Discussion | 38 |
| 3.4.1 | Dynamic Performance of the Controllers with Step Change in Speed: | 39 |
| 3.4.2 | Performance with Generalized Approach of Flux Sharing: | 42 |
| 3.4.3 | Performance of the drive with Proposed Starting Method: | 43 |
| 3.4.4 | Dynamic Performance of the drive with Step Change in Load: | 43 |
| 3.4.5 | Comparison of Proposed Technique with Existing Methods: | 43 |
| | Generalized Comparison | 44 |
| | Performance Comparison | 44 |
| 3.5 | Conclusion | 46 |
| 4 | Minimization of Torque Ripple, Current Ripple, and Switching Loss using Available PWM Techniques | 47 |
| 4.1 | PWM Techniques | 48 |
| 4.1.1 | Conventional Space-Vector PWM (CSVPWM) Technique: | 49 |
| 4.1.2 | Bus-Clamped PWM (BCPWM) Technique: | 50 |
| 4.1.3 | Advanced Bus-Clamped PWM (ABCPWM) Technique: | 52 |
| 4.2 | Estimation of Flux Ripples | 54 |
| 4.2.1 | Estimation of Error Voltage: | 54 |
| 4.2.2 | d -axis flux ripple: | 55 |
| 4.2.3 | q -axis flux ripple: | 57 |
| 4.3 | Minimization of Torque Ripple | 58 |
| 4.3.1 | Analysis of Overall Flux Ripple: | 59 |
| 4.3.2 | Analysis of RMS and Peak-to-Peak Torque Ripple: | 60 |
| | RMS Torque Ripple | 60 |
| | Peak-to-Peak Torque Ripple | 61 |
| 4.3.3 | Results and Discussion: | 61 |
| | Instantaneous Torque Ripple | 61 |
| | Approximate and Exact RMS Torque Ripple | 63 |
| | Harmonic Spectra | 63 |
| | Peak-to-Peak Torque Ripple | 66 |
| 4.4 | Minimization of Current Ripple | 67 |
| 4.4.1 | Analysis of RMS Current Ripple: | 67 |
| 4.4.2 | Analysis and Selection of PWM combinations: | 68 |
| | In Sub-Synchronous Mode | 69 |
| | In Super-Synchronous Mode | 70 |
| | Effect of phase shift γ | 71 |
| 4.4.3 | Results and Discussion: | 72 |
| | Instantaneous Current Ripple | 72 |
| | RMS Current Ripple | 75 |

| | | |
|----------|---|------------|
| 4.5 | Minimization of Switching Loss | 76 |
| 4.5.1 | Switching Loss over a fundamental cycle: | 76 |
| 4.5.2 | Variation of power factor with flux component and load: | 77 |
| 4.5.3 | Variation of switching loss with power factor and load: | 77 |
| 4.5.4 | Experimental Validation: | 78 |
| 4.6 | Conclusion | 80 |
| 5 | Minimization of Torque Ripple using Equivalent 3-Level PWM Technique | 81 |
| 5.1 | Correlation between Topologies of DI-WRIM and DI-OWIM | 82 |
| 5.1.1 | Topology of DI-WRIM drive: | 82 |
| 5.1.2 | Topology of DI-OWIM drive: | 82 |
| 5.1.3 | Resemblance between DI-WRIM and DI-OWIM: | 83 |
| 5.2 | Expression for Torque Ripple | 84 |
| 5.2.1 | In DI-WRIM: | 84 |
| 5.2.2 | In DI-OWIM: | 85 |
| 5.3 | Harmonic Models of DI-WRIM and DI-OWIM | 86 |
| 5.3.1 | DI-WRIM: | 86 |
| 5.3.2 | DI-OWIM: | 86 |
| 5.3.3 | Analogy between DI-WRIM and DI-OWIM | 87 |
| 5.4 | PWM Sequences for Equivalent 3L Overall Flux Ripple | 87 |
| 5.4.1 | In DI-OWIM Topology: | 88 |
| 5.4.2 | In DI-WRIM Topology: | 91 |
| 5.5 | Analysis of Torque Ripple | 92 |
| 5.5.1 | Instantaneous Overall Flux Ripple and Error Voltages: | 92 |
| 5.5.2 | Effect of Phase Difference ' γ ': | 94 |
| 5.6 | Results and Discussion | 96 |
| 5.6.1 | Instantaneous Torque Ripple: | 96 |
| 5.6.2 | Spectra of Torque Ripple and Stator Current: | 97 |
| 5.6.3 | RMS Torque Ripple: | 98 |
| 5.6.4 | Current Ripple: | 99 |
| 5.6.5 | Switching Loss: | 100 |
| 5.6.6 | Comparison between EQ-3L and CSVPWM-ABC30PWMB PWM methods: . . . | 100 |
| 5.7 | Conclusion | 102 |
| 6 | Configuration of Experimental Setup and RFO Control of DI-WRIM | 103 |
| 6.1 | Implementation of FEC and DC-Machine | 104 |
| 6.2 | Implementation of DI-WRIM Drive | 105 |
| 6.3 | Grounding Scheme | 107 |
| 6.4 | Start-up Sequence of Experimental Setup | 107 |
| 6.5 | DI-WRIM drive with Reduced Current Sensors | 108 |
| 6.5.1 | Control Strategy with Reduced Current Sensors: | 108 |
| 6.5.2 | Simulation Results: | 110 |
| 6.5.3 | Experimental Results: | 111 |
| 6.6 | Conclusion | 112 |
| 7 | Conclusions and Future Scope | 113 |
| 7.1 | General | 113 |
| 7.2 | Major Conclusions | 113 |
| 7.2.1 | On the proposed Modelling and Control Technique: | 113 |
| 7.2.2 | On the proposed Ripple Reduction Techniques: | 114 |
| 7.3 | Future Scope | 114 |

| | | |
|----------|--|------------|
| A | Impact of Carrier Interleaving on Torque Ripple | 117 |
| A.1 | Results and Discussion | 118 |
| A.1.1 | Instantaneous Torque Ripple | 118 |
| A.1.2 | RMS Torque Ripple | 118 |
| A.1.3 | Current Ripple | 119 |
| B | Parameters | 121 |
| B.1 | WRIM Ratings | 121 |
| B.2 | DC Machine Ratings | 121 |
| B.3 | Electrical Parameters | 122 |
| B.4 | Mechanical Parameters | 122 |
| | References | 123 |
| | Bio-data and List of Publications/Patents | 127 |

List of Figures

| | | |
|-----|---|----|
| 1.1 | Illustration of DFIG topology. | 1 |
| 1.2 | Illustration of DI-WRIM topology. | 2 |
| 2.1 | Generalized control block diagram of DI-WRIM illustrating both stator and rotor flux oriented control techniques. | 15 |
| 2.2 | Stator and rotor frequency profiles in (i) SFO and (ii) RFO control techniques, for (a) 50 Hz WRIM and (b) scaled 25 Hz WRIM. | 17 |
| 2.3 | Block diagram of (a) inner current loop and (b) outer speed loop. | 19 |
| 2.4 | Vector diagram of WRIM in (a) sub-synchronous and (b) super-synchronous modes, as seen from (i) stator and (ii) rotor reference frames. | 21 |
| 2.5 | Harmonic equivalent circuit of DI-WRIM (a) Generalized circuit, (b)(i) D -axis harmonic circuit in sub- and super- synchronous modes, and (b)(ii) Q -axis harmonic circuit in super-synchronous mode. | 26 |
| 3.1 | Control block diagram of the proposed current oriented control technique. | 33 |
| 3.2 | (i) Illustration of \bar{i}_s , \bar{i}_r , and \bar{i}_m and, their variation with load, in (a) (d_1 - q_1) frame, (b) (d_2 - q_2), and (c) (d_3 - q_3) frame. | 35 |
| 3.3 | Trace of \bar{i}_s , \bar{i}_r , and \bar{i}_m , with (a) equal and (b) unequal flux sharing, using proposed starting method. | 37 |
| 3.4 | Experimental results illustrating the performance of the drive, when speed reference is changed from (i) 0 to 1 p.u. ($t = 0$ s) and (ii) 1 p.u. to -1 p.u. ($t = 5$ s), with the machine is operated in sub- and super- synchronous modes and $K_m = 0.5$. Response of (a) d_1 -axis stator, (b) d_2 -axis rotor, and (c) q_1 - and q_2 - axes current controllers. | 38 |
| 3.5 | Experimentally obtained (a) d_1q_1 axes stator and (b) d_2q_2 axes rotor voltage references and, (c) measured stator and rotor line currents, when speed reference is changed from (i) 0 to 1 p.u. ($t = 0$ s) and (ii) 1 p.u. to -1 p.u. ($t = 5$ s), with machine operated in sub- and super- synchronous modes and $K_m = 0.5$ | 39 |
| 3.6 | Experimentally obtained (a) Stator and rotor frequency profiles, (b) (α - β) stator and (c) (a - b) rotor currents, when speed reference is changed from (i) 0 to 1 p.u. ($t = 0$ s) and (ii) 1 p.u. to -1 p.u. ($t = 5$ s), with machine operated in sub- and super- synchronous modes and $K_m = 0.5$ | 40 |
| 3.7 | Experimental results illustrating the performance of the drive, when speed reference is changed from (i) 0 to 1 p.u. ($t = 0$ s) and (ii) 1 p.u. to -1 p.u. ($t = 5$ s), with the machine operated only in super-synchronous mode and $K_m = 0.5$. (a) Response of d_1 -axis stator current controller, (b) measured stator and rotor line currents, and (c) stator and rotor frequency profiles, during the transients. | 41 |
| 3.8 | Illustration of performance of drive, with step change in speed from (i) 0 to 1 p.u. ($t = 0$ s) and (ii) 1 p.u. to -1 p.u. ($t = 5$ s) and $K_m = 0.75$. Response of (a) d -axis stator and (b) d_1 -axis rotor current controllers. (c) Response of current controllers, when K_m changes from 0.5 to 0.75. | 42 |

| | | |
|------|---|----|
| 3.9 | Starting response of the drive with proposed starting method. (a) Response of d_1 -axis stator current controller, (b) stator and rotor frequency profiles, (c) measured stator and rotor currents, and (d) load angle (δ_c^*). | 42 |
| 3.10 | Response of the controllers with step change in load from 0 to 0.75 p.u. Response of (a) d_1 -axis stator and (b) d_1 -axis rotor current controllers, (c) measured stator and rotor currents, and (d) load angle (δ_c^*). | 43 |
| 3.11 | (a) Response of current controllers and (b) Measured stator and rotor line currents, without feed-forward compensation and, Output of the d_1 -axis stator controller ($v_{sd,con}$) (a) with and (b) without feed-forward compensation, when w_e^* is changed from 0 to 1 p.u. and (i) 1 p.u. to -1 p.u. | 45 |
| 4.1 | (a) Topology of 2-level converter and (b) 2-level space vector polygon. | 48 |
| 4.2 | Switching Sequences for (a) CSVPWM and (b) BCPWM techniques. | 50 |
| 4.3 | Switching Sequences for ABCPWM techniques. | 52 |
| 4.4 | (a) Illustration of reference and error voltages. $\hat{\psi}_d$ of (b) S-0127 and S-7210 and, (c) S-012 and S-721 switching sequences, at positions α and $60 - \alpha$ | 56 |
| 4.4 | $\hat{\psi}_d$ of (d) S-7212 and S-0121 and, (e) S-2721 and S-1012 switching sequences, at positions α and $60 - \alpha$ | 56 |
| 4.5 | (a) Illustration of reference and error voltages. $\hat{\psi}_q$ of (b) S-0127 and S-7210 and (c) S-012 and S-721 switching sequences, at positions α and $60 - \alpha$ | 58 |
| 4.5 | $\hat{\psi}_q$ of (d) S-7212 and S-0121, and (e) S-2721 and S-1012 switching sequences, at positions α and $60 - \alpha$ | 58 |
| 4.6 | (a) Variation of $(\psi_{sQ} + \psi_{rQ1})$ ripple and (b) $(2\psi_{sQ}\psi_{rQ1})$, for (i) CSVPWM-CSVPWM, (ii) CSVPWM-ABC30PWMA, and (iii) CSVPWM-ABC30PWMB PWM combinations, applied to stator-rotor converters, at $V_s = V_r = 0.81V_{dc}$, $T_s = 500\mu s$ | 59 |
| 4.7 | (a) Variation of square of $(\psi_{q,rms})$ ripple and (b) Variation of term ' P_q ' over a sector (T) with F_e , in super-synchronous mode. | 60 |
| 4.8 | (a) Analytically evaluated, (b) simulated and (c) experimentally obtained instantaneous torque ripple, for stator-rotor (i) CSVPWM-CSVPWM, (ii) CSVPWM-ABC30PWMA and (iii) CSVPWM-ABC30PWMB PWM combinations, at $F_e = 45$ Hz, $F_{sw} = 1$ kHz, and no load. | 62 |
| 4.9 | (a) Variation of RMS Overall ripple, (b) Variation of term ' P ' over a sector with α_r , at $\alpha_s = 5^\circ$ | 62 |
| 4.10 | Exact and approximate RMS torque ripple over a sector, for different PWM combinations, at no load. | 63 |
| 4.11 | (a) Analytically evaluated ($F_e \geq 17.5$ Hz), (b) simulated and (c) experimentally obtained RMS torque ripple over a sector for stator-rotor (i) CSVPWM-CSVPWM, (ii) CSVPWM-ABC30PWMA and (iii) CSVPWM-ABC30PWMB PWM combinations at no load, $F_{sw} = 1$ kHz. | 64 |
| 4.12 | Harmonic spectra of experimentally obtained (a) Torque ripple, (b) stator current (in $(\alpha-\beta)$ frame) and (c) rotor current (in $(a-b)$ frame) for PWM combinations (i) CSVPWM-CSVPWM and (ii) CSVPWM-ABC30PWMB (proposed combination) at $F_e = 45$ Hz, $F_{sw} = 1$ kHz, and no load. | 65 |
| 4.13 | Experimentally obtained peak-to-peak torque ripple for different PWM combinations, at no load, $F_{sw} = 1$ kHz. | 66 |
| 4.14 | Variation of (a) d -axis RMS flux ripple and (b) q -axis RMS flux ripple with F_s or F_r | 68 |
| 4.15 | Instantaneous variation of (a) D -axis and (b) Q -axis overall flux ripples, for PWM combinations (i) CSVPWM-CSVPWM, (ii) CSVPWM-ABC30PWMB, (iii) ABC30PWMA-ABC30PWMA, (iv) ABC30PWMA-BCPWMMi and (v) BCPWMM-BCPWMMi, at $V_s = V_r = 0.81V_{dc}$, $\alpha_s = 5^\circ$ and $T_s = 500\mu s$ | 69 |

| | | |
|------|---|----|
| 4.16 | Instantaneous variation of (a) $(2\hat{\psi}_{sD}\hat{\psi}_{rD_1})$ and (b) $(2\hat{\psi}_{sQ}\hat{\psi}_{rQ_1})$, for PWM combinations (i) CSVPWM-CSVPWM, (ii) CSVPWM-ABC30PWMB, (iii) ABC30PWMA-ABC30PWMA, (iv) ABC30PWMA-BCPWMMi and (v) BCPWMM-BCPWMMi, at $V_s = V_r = 0.81V_{dc}$, $\alpha_s = 5^\circ$ and $T_s = 500\mu s$ | 71 |
| 4.17 | Analytically obtained variation of (a) P_d and (b) P_q for PWM combinations (i) CSVPWM-CSVPWM, (ii) CSVPWM-ABC30PWMB, (iii) ABC30PWMA-ABC30PWMA, (iv) ABC30PWMA-BCPWMMi and (v) BCPWMM-BCPWMMi with F_e at $\alpha_s = 5^\circ$, $F_{sw} = 1$ kHz. | 72 |
| 4.18 | Instantaneous waveforms of (a) experimentally obtained D_1Q_1 axes stator and rotor current ripples and (b) measured stator and rotor currents, for PWM combinations (i) CSVPWM-CSVPWM, (ii) CSVPWM-ABC30PWMB, (iii) ABC30PWMA-ABC30PWMA, (iv) ABC30PWMA-BCPWMMi and (v) BCPWMM-BCPWMMi, at $F_e = 42.5$ Hz, $F_{sw} = 1$ kHz, and no-load. | 73 |
| 4.19 | Variation of (a) analytical ($F_e \geq 17.5$ Hz) at different α_r , constant $\alpha_s = 5^\circ$, simulation (b) without and (c) with dead-time and, (d) experimentally obtained RMS current ripple for (i) CSVPWM-CSVPWM, (ii) CSVPWM-ABC30PWMB, (iii) ABC30PWMA-ABC30PWMA for $F_e < 17.5$ Hz and ABC30PWMA-ABC30PWMA for $F_e \geq 17.5$ Hz, (iv) ABC30PWMA-BCPWMMi and (v) BCPWMM-BCPWMMi combinations with F_e at no load, $F_{sw} = 1$ kHz. | 74 |
| 4.20 | Variation of P_{sw} for a single converter with power factor angle, for different PWM techniques. | 76 |
| 4.21 | Variation of P_{sw} for (i) ABC30PWMA-ABC30PWMA, (ii) ABC60PWMA-ABC60PWMA, (iii) ABC30PWMA-BCPWMMi, and (iv) ABC60PWMA-BCPWMMi combinations with I_{rD_1} at different load. | 78 |
| 4.22 | Temperature of stator and rotor VSCs, for CSVPWM-CSVPWM combination, at different switching frequencies, $F_e = 30$ Hz, 50% load. | 78 |
| 5.1 | Illustration of (a) DI-WRIM, (b) DI-OWIM, and (c) 3L NPC fed SQIM topologies. | 81 |
| 5.2 | Illustration of (a) Sub-hexagonal and (b) Decoupled space vector PWM switching techniques for DI-OWIM topology. | 82 |
| 5.3 | Harmonic equivalent circuit of (a) DI-WRIM and (b) DI-OWIM drives. | 86 |
| 5.4 | Illustration of 3-level Space vector polygon. | 87 |
| 5.5 | Illustration of (a) 2L-Space vector polygon and (b) reference vector in 3L-SVP. | 88 |
| 5.6 | 2L-SVP illustrating the sector division and, equivalent 2L sequences for VSC-S, in each sector. | 92 |
| 5.7 | Instantaneous (i) $V_{sQ, err}$, (ii) $V_{rQ_2, err}$, and (iii) $(V_{sQ, err} + V_{rQ_2, err})$ of DI-WRIM and, (iv) $V_{sQ, err}$ of 3L-SQIM, for (a) CSVPWM-CSVPWM, (b) CSVPWM-ABC30PWMB, and (c) EQ-3L-CSVPWM combinations, at $\alpha_s = \alpha_r = 10^\circ$, $V_s = V_r = 0.76V_{dc}$ [$F_e = 45$ Hz], and $T_s = 333.33\mu s$ | 93 |
| 5.8 | Instantaneous (i) $\hat{\psi}_{sQ}$, (ii) $\hat{\psi}_{rQ_2}$, and (iii) $(\hat{\psi}_{sq} + \hat{\psi}_{rQ_2})$ of DI-WRIM and, (iv) $\hat{\psi}_{sQ}$ of 3L-SQIM, for (a) 2L CSVPWM-CSVPWM, (b) 2L CSVPWM-ABC30PWMB [12], and (c) EQ-3L-CSVPWM combinations, at different α_r , $\alpha_s = 10^\circ$, $V_s = V_r = 0.76V_{dc}$ [$F_e = 45$ Hz], and $T_s = 333.33\mu s$ | 94 |
| 5.9 | Variation of (a) $\hat{\psi}_{Q, rms}$ and (b) P with F_e (Hz), for (i) CSVPWM-CSVPWM, (ii) CSVPWM-ABC30PWMB, (iii) EQ-3L-CSVPWM, and (iv) EQ-3L-CSVPWM-Hy combinations. | 95 |
| 5.10 | Instantaneous (i) $\hat{\psi}_{sQ}$, (ii) $\hat{\psi}_{rQ_2}$, and (iii) $(\hat{\psi}_{sQ} + \hat{\psi}_{rQ_2})$, for (a) EQ-3L-CSVPWM and (b) EQ-3L-CSVPWM-Hy combinations, at different α_r , $\alpha_s = 10^\circ$, $V_s = V_r = 0.42V_{dc}$ [$F_e = 25$ Hz], and $T_s = 333.33\mu s$ | 96 |
| 5.11 | (a) Analytical, (b) simulated, and (c) experimentally obtained torque ripple waveforms, for (i) 2L CSVPWM-CSVPWM, (ii) 2L CSVPWM-ABC30PWMB, and (iii) EQ-3L-CSVPWM combinations, at $F_e = 45$ Hz, no load, and $F_{sw} = 1.5$ kHz. | 97 |
| 5.12 | Measured harmonic spectra of (d) torque ripple and (e) stator current, for (i) CSVPWM-CSVPWM, (ii) CSVPWM-ABC30PWMB, and (iii) EQ-3L-CSVPWM combinations, at $F_e = 45$ Hz, no load, and $F_{sw} = 1.5$ kHz. | 97 |

| | | |
|------|--|-----|
| 5.13 | Variation of (a) Analytically estimated at $\alpha_s = 10^\circ$ and different α_r and (b) experimentally obtained RMS current ripple with F_e , for (i) CSVPWM-CSVPWM and (ii) CSVPWM-ABC30PWMB, (iii) EQ-3L-CSVPWM, and (iv) EQ-3L-CSVPWM-Hy PWM combinations, at no load and $F_{sw} = 1.5$ kHz. | 98 |
| 5.14 | Variation of (a) Analytically estimated at $\alpha_s = 10^\circ$ and different α_r and (b) experimentally obtained RMS current ripple with F_e , for (i) CSVPWM-CSVPWM and (ii) CSVPWM-ABC30PWMB, (iii) EQ-3L-CSVPWM, and (iv) EQ-3L-CSVPWM-Hy PWM combinations, at no load and $F_{sw} = 1.5$ kHz. | 99 |
| 5.15 | Variation of P_{sw} , (a) with power factor angle for a single VSC and different PWM techniques and, (b) with I_{rD_1} of DI-WRIM, at different load, for (i) CSVPWM-ABC30PWMB and (ii) EQ-3L-CSVPWM combinations. | 100 |
| 5.16 | Variation of p.u. reduction of proposed EQ-3L-CSVPWM-Hy combination, with respect to (i) CSVPWM-CSVPWM and (ii) CSVPWM-ABC30PWMB. | 101 |
| 6.1 | Block diagram of experimental setup illustrating various hardware components. | 103 |
| 6.2 | Picture of the experimental setup illustrating various hardware components. | 106 |
| 6.3 | Simulation results illustrating (a) reference, estimated and actual rotor speed, (b) M_d and i_{sQ_1} , (c) stator and rotor frequencies, and rotor speed in Hz, (i) at $t = 6$ s, and (ii) at $t = 12$ s, (d)(i) estimated $\cos(\rho)$, $\sin(\rho)$, and (ii) $\cos(\rho - \epsilon)$, $\sin(\rho - \epsilon)$, at $t = 6$ s, (e) stator currents $(I_{s\alpha}, I_{s\beta})$, (i) at $t = 6$ s. | 109 |
| 6.4 | Simulation results illustrating (a) estimated and measured i_{rQ_1} , (b) estimated and measured i_{rD_1} and (c) estimated and measured ψ_{rD_1} | 110 |
| 6.5 | Experimental results illustrating (a) reference (ω_m^*), estimated rotor speed (ω_m), and i_{sQ_1} , (i) at $t = 8$ s, (b) stator currents $(I_{s\alpha}, I_{s\beta})$, (i) at $t = 8$ s, (c) stator and rotor frequencies, and rotor speed in Hz, (i) at $t = 8$ s, and (ii) at $t = 14$ s, and (d)(i) estimated $\cos(\rho)$, $\sin(\rho)$, and (d)(ii) $\cos(\rho - \epsilon)$, $\sin(\rho - \epsilon)$, at $t = 8$ s. | 111 |
| 6.6 | Experimental results illustrating error in estimated and measured (i) i_{rD_1} and i_{rQ_1} , (ii) at $t = 8$ s, and (iii) at $t = 14$ s. | 112 |
| A.1 | Instantaneous variation of Q -axis flux ripple, at different carrier interleaving angle of (a) 0° and (b) 90° , for CSVPWM, at different α , $ V_{ref} = 0.76V_{dc}$, and $T_{sw} = 1$ ms. | 117 |
| A.2 | Analytically estimated torque ripple, at different carrier interleaving angle of (a) 0° and (b) 90° , for CSVPWM-CSVPWM combination, at $\alpha_s = 0^\circ$ and different α_r , $ V_{ref} = 0.76V_{dc}$, and $T_{sw} = 1$ ms. | 118 |
| A.3 | (i) Analytically obtained, (ii) simulated, and (iii) experimentally obtained instantaneous torque ripple waveforms, for CSVPWM-CSVPWM combination, carrier interleaving angle of (a) 0° and (b) 90° , at rotor speed $F_e = 45$ Hz. | 119 |
| A.4 | Variation of (i) Analytically obtained ($F_e \geq 17.5$ Hz), (ii) simulated, and (iii) experimentally obtained RMS torque ripple, with rotor electrical speed (F_e), for CSVPWM-CSVPWM combination, carrier interleaving angle of (a) 0° and (b) 90° , at rotor speed $F_e = 45$ Hz. | 119 |
| A.5 | Variation of (i) Analytically obtained ($F_e \geq 17.5$ Hz) and (ii) experimentally obtained RMS current ripple, with rotor electrical speed (F_e), for CSVPWM-CSVPWM combination, carrier interleaving angle of (a) 0° and (b) 90° , at rotor speed $F_e = 45$ Hz. | 120 |

List of Tables

| | | |
|-----|---|-----|
| 3.1 | Comparison of Proposed Technique with Existing Methods | 44 |
| 4.1 | Switching Sequences for CSVPWM Technique, in all Six Sectors. | 49 |
| 4.2 | Switching Sequences for BCPWM Techniques, in all Six Sectors. | 51 |
| 4.3 | Switching sequences for ABCPWM Techniques | 53 |
| 4.4 | Modified Reference Voltages for ABC30PWMA and ABC30PWMB in sector-1. | 53 |
| 4.5 | RMS Torque Ripple at Different Load. | 64 |
| 4.6 | RMS Current Ripple at Different Load, $F_e = 30$ Hz. | 75 |
| 4.7 | Measured temperature rise (ΔT_r) for different PWM combinations, at $F_e = 30$ Hz and full flux fed from stator terminals. | 79 |
| 4.8 | Estimated temperature rise due to conduction loss (ΔT_{con}) and switching loss (ΔT_{swt}), for different PWM combinations. | 79 |
| 5.1 | 3L Switching States using 2L States of VSC-1 and VSC-2 | 88 |
| 5.2 | 2L Sequences for Equivalent 3L Operation. | 89 |
| 5.3 | Dwell times of 2L states in terms of 3L dwell times. | 90 |
| 5.4 | Dwell times of 3L states in terms of 2L dwell times. | 91 |
| 5.5 | Modified 2L reference voltages for S-10127 and S-27210 sequences. | 91 |
| 5.6 | RMS Torque Ripple at different Load, $F_e = 45$ Hz. | 99 |
| 5.7 | Comparison of proposed PWM with existing PWM. | 101 |

Nomenclature

| Symbol | Definition |
|------------------------------------|---|
| <u>Different Reference Frames:</u> | |
| $(\alpha-\beta)$ | Stationary reference frame |
| $(a-b)$ | Rotor reference frame |
| $(d-q)$ | Synchronously rotating arbitrary reference frame |
| $(D-Q)$ | Stator flux reference frame as seen from $(\alpha-\beta)$ |
| (D_1-Q_1) | Rotor flux reference frame as seen from $(\alpha-\beta)$ |
| (D_2-Q_2) | Rotor flux reference frame as seen from $(a-b)$ |
| (D_3-Q_3) | Air-gap flux reference frame as seen from $(a-b)$ |
| (d_1-q_1) | Stator current reference frame as seen from $(\alpha-\beta)$ |
| (d_2-q_2) | Rotor current reference frame as seen from $(a-b)$ |
| (d_3-q_3) | Magnetizing current reference frame as seen from $(\alpha-\beta)$ |
| <u>Different Variables:</u> | |
| \bar{v}_s | Stator voltage vector in $(\alpha-\beta)$ |
| \bar{v}_r | Rotor voltage vector in $(a-b)$ |
| \bar{i}_s | Stator current vector in $(\alpha-\beta)$ |
| \bar{i}_r | Rotor current vector in $(a-b)$ |
| $\bar{\psi}_s$ | Stator flux vector in $(\alpha-\beta)$ |
| $\bar{\psi}_r$ | Rotor flux vector in $(a-b)$ |
| v_1^*, v_2^*, v_3^* | Three phase voltage references |
| $v_{max}^*, v_{mid}^*, v_{min}^*$ | Maximum, middle, and minimum of (v_1^*, v_2^*, v_3^*) |
| m_d | Fundamental generated torque |
| ω_s | Stator angular frequency |
| ω_r | Rotor angular frequency |
| ω_e | Rotor electrical angular frequency |
| F_s | Stator frequency |
| F_r | Rotor frequency |
| F_e | Rotor electrical frequency |
| ω_m | Rotor mechanical angular frequency |
| V_{dc} | Dc-link voltage |
| α_s | Angle between \bar{v}_s and α -axis |
| α_r | Angle between \bar{v}_r and a -axis |
| θ_s | Angle between \bar{i}_s and α -axis |

| | |
|------------|--|
| θ_r | Angle between \bar{i}_r and a -axis |
| μ | Angle between $\bar{\psi}_s$ and α -axis |
| μ' | Angle between $\bar{\psi}_{sr}$ and a -axis |
| ρ | Angle between $\bar{\psi}_{rs}$ and α -axis |
| ρ' | Angle between $\bar{\psi}_r$ and a -axis |
| δ | Load angle between stator and rotor fluxes |
| δ_c | Load angle between stator and rotor currents |
| γ | Angle between \bar{v}_s and \bar{v}_r |

| | |
|-----------------|---|
| Subscript 'rs' | Rotor variable referred to (α - β) |
| Subscript 'sr' | Stator variable referred to (a - b) |
| Subscript 'xy' | 'x' variable along y -axis |
| Superscript '^' | Represents the ripple quantity |
| Superscript '*' | Represents the reference or set quantity |

Constants:

| | |
|------------|---|
| L_s | Stator self inductance |
| L_r | Rotor self inductance |
| L_{ls} | Stator leakage inductance |
| L_{lr} | Rotor leakage inductance |
| L_o | Magnetizing inductance |
| L_g | Grid inductance |
| R_s | Stator resistance |
| R_r | Rotor resistance |
| R_g | Grid inductance's resistance |
| σ_s | Stator leakage factor |
| σ_r | Rotor leakage factor |
| σ | Total leakage factor ($1 - \frac{L_o^2}{L_s L_r}$) |
| J | Moment of inertia |
| B | Friction Co-efficient |
| P | No. of poles |
| S0-S7 | Switching states or vectors of a 2-level space vector polygon |
| T_1 | Dwell time of active vector S1 |
| T_2 | Dwell time of active vector S2 |
| T_z | Dwell time of inactive vector S0 or S7 |
| T_c | Carrier period |
| T_s | Sub-cycle or half of carrier period |
| T_{sam} | Sampling period |
| T_{inv} | Converter delay |
| T_m | Mechanical time constant |
| T_f | Filter time constant |

| | |
|-----------|----------------------------------|
| F_{sw} | Switching frequency |
| F_{sam} | Sampling frequency |
| K_{pi} | Inner-loop proportional constant |
| T_{ci} | Inner-loop PI-C time constant |
| K_{po} | Outer-loop proportional constant |
| T_{co} | Outer-loop PI-C time constant |